ELSEVIER

Chemical Engineering Science 60 (2005) 6551–6563

Chemical Engineering Science

www.elsevier.com/locate/ces

Appraisal of three-dimensional numerical simulation for sub-micron particle deposition in a micro-porous ceramic filter

Fabio Sbrizzai[a], Paolo Faraldi[b], Alfredo Soldati[a,*]

[a]*Centro Interdipartimentale di Fluidodinamica e Idraulica and Dipartimento di Energetica e Mecchine, Università degli Studi di Udine, Udine 33100, Italy*
[b]*Advanced Process Technologies - Centro Ricerche FIAT (CRF), Strada Torino 50, 10043 Orbassano (TO), Italy*

Received 27 October 2004; received in revised form 21 March 2005; accepted 13 May 2005
Available online 14 July 2005

Abstract

A computational, three-dimensional approach to investigate the behavior of diesel soot particles in the micro-channels of a wall-flow, porous-ceramic particulate filter is presented. Particle size examined is in the PM2.5 range. The flow field is simulated with a finite-volume Navier–Stokes solver and the Ergun equation is used to model the porous material. The permeability coefficients were obtained by fitting experimental data. Particle flow, dispersion, deposition and wall–particle interactions are investigated tracking large swarms of 2 and 0.2 μm diameter particles in a Lagrangian frame of reference. Particle dynamics included rarefied gas hypotheses (the Knudsen number being larger than unity) and bounce/capture models based on impact kinetic energy loss. The influence of gas molecules–particle interaction on overall particle behavior is also examined by including Brownian motion and partial slip in particle equation of motion. Simulations help to highlight three-dimensional non-uniform particle deposition, mainly due to flow distribution in the micro-channel. All particles deposit onto the porous filter wall following the distribution of the through-wall velocity. The larger, 2 μm, particles show a larger tendency to deposit at the end of the filter. Due to the flow contraction at the inlet, virtually no particle deposit in the inlet section of the filter. Reasons for the scarce influence on particle deposition due to particle-flow slip and Brownian motion are given.

Keywords: Nanoparticles; Micro-porous filter; Deposition; Numerical simulation

1. Introduction

The presence in the environment of particles with size ranging from 10 nm to 10 μm (known in technical literature as PM10) has a profound impact on human health due to their tendency to remain trapped in the inner respiratory ways causing a variety of lung-disease typologies. It is known that in urban environment a significant amount of these micro-particles is produced by diesel engines which are specifically responsible for the emission of soot with size ranging in the sub-micron scale, with an average diameter of about 150–200 nm (part of the so-called PM2.5, i.e., particles with diameter smaller than 2.5 μm). The intrinsic lung-damaging effect of the diesel soot particles is further increased by the presence of policyclic aromatic hydrocarbons and nitro compounds adsorbed on their surface (Saracco et al., 1999), which form a soluble organic fraction (SOF) responsible for mutagens and carcinogenic effects (Kagawa, 2002; Fino et al., 2003).

Diesel soot production can be reduced, for instance, by optimizing fuel combustion or by filtering the post-combustions gases. Among other filtering techniques, a suitable, low-cost way to reduce diesel particulate emissions down to acceptable concentrations (e.g., less than 0.025 g/km, as per the 2005 EU regulations—Euro 4) is the use of particulate traps placed in the exhaust line of vehicles, as shown in Fig. 1(a). We will examine in particular the broadly used wall-flow ceramic filters. The working principle is sketched in Fig. 1(b) and it is based on the permeability properties of porous ceramics, such as *silicon*

* Corresponding author. Tel.: +39 0432 558020; fax: +39 0432 558027.
E-mail address: soldati@uniud.it (A. Soldati).

0009-2509/$ - see front matter © 2005 Elsevier Ltd. All rights reserved.
doi:10.1016/j.ces.2005.05.038

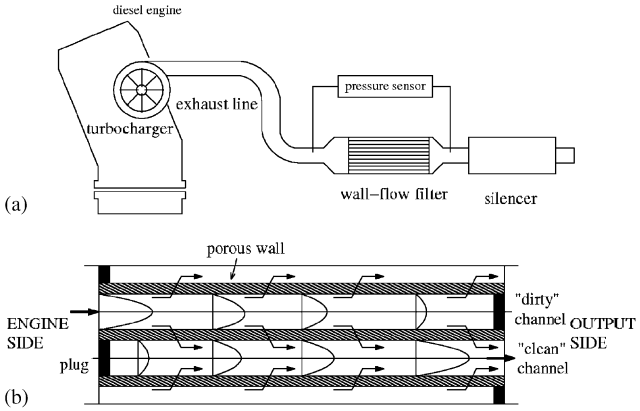

Fig. 1. Schematic of the experimental apparatus used to measure the gas parameters in the exhaust line of a diesel engine equipped with a wall-flow filter (a). Working principle of the wall-flow filter (b).

carbide (*SiC*) and *cordierite* ($2MgO \cdot 2Al_2O_3 \cdot 5SiO_2$). The structure of these materials is characterized by a high surface concentration of $O(10\,\mu m)$ pores through which the particle-laden flow is driven thus ensuring particle adsorption at the ceramic walls. Additives are usually added to fuel and to filter walls to reduce soot combustion temperature avoiding excessive pressure drop across the filter caused by particulate accumulation and thermal stresses due to particulate burn-off (Ambrogio et al., 2001).

A continuing effort of the research community aims at producing optimized diesel traps with the highest filtering efficiency and the lowest pressure drop. Specifically, attention is paid to the filter regeneration cycle which is a strong function of particle deposition mechanisms. Briefly, the filter must be re-generated (the deposited soot is burnt) to avoid large pressure drop (detrimental for engine performance) and loss of filtering efficiency. However, since re-generation is a highly polluting phase, the environmentally optimal cycle length must be identified. During the filter cycle, particles driven through the filter deposit, foul and eventually plug specific filter areas, giving rise to a spatially non-uniform deposition. Optimal filtering efficiency leading to longer regeneration cycles would be ensured (i) by a uniform particle distribution in the filter cross-section, so that filtering load is distributed uniformly among the micro-channels (Sbrizzai et al., 2004) and (ii) by uniform particle deposition inside each single micro-channel. To understand and possibly optimize particle deposition inside micro-channels we have to rely on accurate local measurements and on accurate and reliable three-dimensional simulations. Measurements are hard and costly (Saracco et al., 1999) and literature shows a surprising lack of sophisticated simulations of three-dimensional particle behavior inside the flow field developing in the porous walls micro-channels characterizing the ceramic filter. Precisely, this lack of literature is the motivation for our study.

Particle deposition is dominated by the flow field, the characteristics of which have been addressed by the scientific literature only in a macroscopic way in a large number of experimental works characterizing the macro-scale features of particulate filtration (see, e.g., Saracco et al., 1999; Ambrogio et al., 2001, 2002; Fino et al., 2003). Specific models using balance equations to predict filter efficiency have been developed, for instance, by Ambrogio et al. (2001), who use balance equations to predict filter efficiency as a function of the different terms corresponding to particle impaction, interception, Brownian diffusion, soot accumulation and other second-order terms. We notice however, that currently proposed models do not allow insight of the three-dimensional features of the flow field leading to non-uniform deposition, and may not be used for optimizing filtering esteem parameters.

In this work we exploit numerical models to investigate the behavior of sub-micron particles dispersed in the three-dimensional flow field which develops in the smallest micro-channel working unit of a particulate trap. In particular, we want to identify a suitable way to predict accurately particle deposition in the trap by using a numerical solution of the Navier–Stokes equations for the fluid and the Lagrangian tracking method. Navier–Stokes equations are solved by a finite-volume commercial code, and Ergun equation is used to reproduce the characteristics of the porous materials separating the channels. Permeability coefficients α and β in the Ergun equation are obtained through an adjustment procedure and fitted to experimental data (i.e., flowrate vs. pressure drop) measured on the real filter.

The particulate trap object of our investigation is that described by Saracco et al. (1999) and Fino et al. (2003) which is broadly employed in the automotive industry. Specifically, the configuration presented is that of the exhaust line of a category of cars produced by FIAT Auto. The filter is made by a periodic arrangement of longitudinal, square-section micro-channels of $O(1\,mm)$ side, into which the particle-laden flow is driven, as shown in Fig. 1(b). Ceramic plugs are placed in a chessboard arrangement either at the end or at the beginning of each channel, so as the exhaust gas flow is forced to cross the porous-ceramic walls and soot particles deposit in the micro-pore network of the walls.

Sub-micron particles are characterized by a size which scales with the mean free path λ of molecules of the high-temperature carrier gas. In the examined cases of $0.2\,\mu m$ particles, the *Knudsen number Kn*, that is the ratio between the mean free path of the gas molecules and the particle diameter, is 0.52. Specific particle–gas interaction modelling is required to take into account both drag coefficient modification, through the Cunningham correction factor (Li and Ahmadi, 1993; Crowe et al., 1998; Fan and Ahmadi, 1995, 2000; Shams et al., 2000) and, being the kinetic energy of a gas molecule high enough to impact on particle trajectory, a Brownian force term (Li and Ahmadi, 1993; Fan and Ahmadi, 1995, 2000; Shams et al., 2000). Also, particle–wall interactions are modelled by means of a restitution coefficient derived on the basis of the kinetic energy loss at the impact (Wall et al., 1990; Johnson and Pollock, 1994; Dahneke, 1995; Brach and Dunn, 1995, 1998 among others).

2. Methodology

2.1. Flow field simulation

Reynolds number based on the average velocity of the exhaust gas and on the channel side gives a value of ~ 200, in the range of laminar flow regime. To obtain an accurate numerical solution of the flow field, we used a commercial, finite-volume Navier–Stokes solver (Star-CD). Diesel engine exhaust smoke systems are preceded by a turbocharger and a long pipe. We can thus, in a first approximation, neglect flow oscillations and solve the steady-state flow field. The equations solved are mass balance:

$$\frac{\partial u_i}{\partial x_i} = 0 \tag{1}$$

and momentum balance:

$$u_j \frac{\partial u_i}{\partial x_j} = -\frac{\partial P^*}{\partial x_i} + \nu \frac{\partial^2 u_i}{\partial x_j^2} \tag{2}$$

written in incompressible form due to limited pressure drop, which is small enough to make compressibility effects negligible. In Eq. (2), P^* is the kinematic pressure term P/ρ, and P is the time-averaged pressure field. Equations are solved using the SIMPLE algorithm.

Flow field is calculated in a limited region of the filter, representing an elementary portion of it which, periodically reproduced in the x and y directions, forms the overall structure. This element is sketched in Fig. 2. It provides a periodic arrangement of longitudinal square-section micro-channels with side l of 1.4 mm. As shown in Fig. 2 domain inlet, at the center of which the origin of reference frame is located, lies at about 36 channel sides upstream of the filter face to make flow field in proximity of the filter independent from inlet conditions. For the same reason, outlet is placed at 33 channel sides downstream of the filter exit. The overall length of the filter is $L = 181l$, whereas the length of the domain is $250l$. Computational domain is discretized into $44 \times 44 \times 159$ hexaedric finite-volumes (giving an overall amount of 307 824 cells) in the spanwise x and y directions and in the streamwise z, respectively. For clarity, the sub-division along the z direction is not shown in Fig. 2. Dark-gray cells represent fluid conditions, whereas light-gray cells are used to model the porous walls. A grid refinement is visible in correspondence of the interface between fluid cells and porous cells where larger velocity gradients were found in preliminary simulations.

Two of the four channels are plugged at entrance, with ceramic plugs 1–2 channel sides long. Similar plugs are placed at the end of the other two channels, forcing the flow to cross the porous ceramic and to trap particles on the surface of the filter walls (thickness of which is s=0.38 mm). Channels with a plug placed at the entrance are crossed by a particle-free gas stream (since particles have been captured by the wall, in the adjacent channel) and will be referred to as *clean channels*, whereas the channels plugged at the end, containing all particles, will be referred to as *dirty channels* hereinafter.

2.2. Flow boundary conditions

Appropriate boundary conditions are applied to domain boundaries to reproduce faithfully the working conditions of the filter. As shown in Fig. 2, an inlet condition is placed in the far upstream boundary, normal to z-axis. It provides a velocity of 3 m/s, uniform along x and y directions and parallel to z-axis. At the opposite boundary mass balance conservation is ensured by an outlet condition.

As mentioned earlier, being the domain represented in Fig. 2 an elementary part of a periodic arrangement, periodic conditions are applied to all boundaries perpendicular to x- and y-axes. This means that flow conditions found at one lateral side of the domain are re-introduced at opposite side, both in x and in y directions. Finally, a no-slip and no-cross boundary condition is applied to all solid surfaces (e.g., the plugs).

2.3. Porosity modelling against experiments

To obtain a realistic representation of working conditions, correct values for the porosity parameters must be determined. The porosity index of the ceramic used to build the filter was experimentally determined and its value, defined as

$$\varepsilon = \frac{\text{volume void fraction}}{\text{overall volume}} \tag{3}$$

is $\varepsilon = 0.45$.

The flow field through the porous walls is modelled by the Darcy equation, giving a distributed pressure loss described by Eq. (4),

$$\vec{u} = -\frac{k}{\mu} \nabla P \tag{4}$$

in which k_i is the permeability, μ is the fluid viscosity and P is the static pressure. $\vec{u}$ is the superficial velocity vector.

The permeability value was obtained as:

$$k_i = \alpha_i |\vec{u}| + \beta_i \tag{5}$$

α_i and β_i being the *permeability coefficients*.

In the present case, k_i is the same for all directions ($k_i = k$), i.e., the medium is isotropically porous and the Ergun

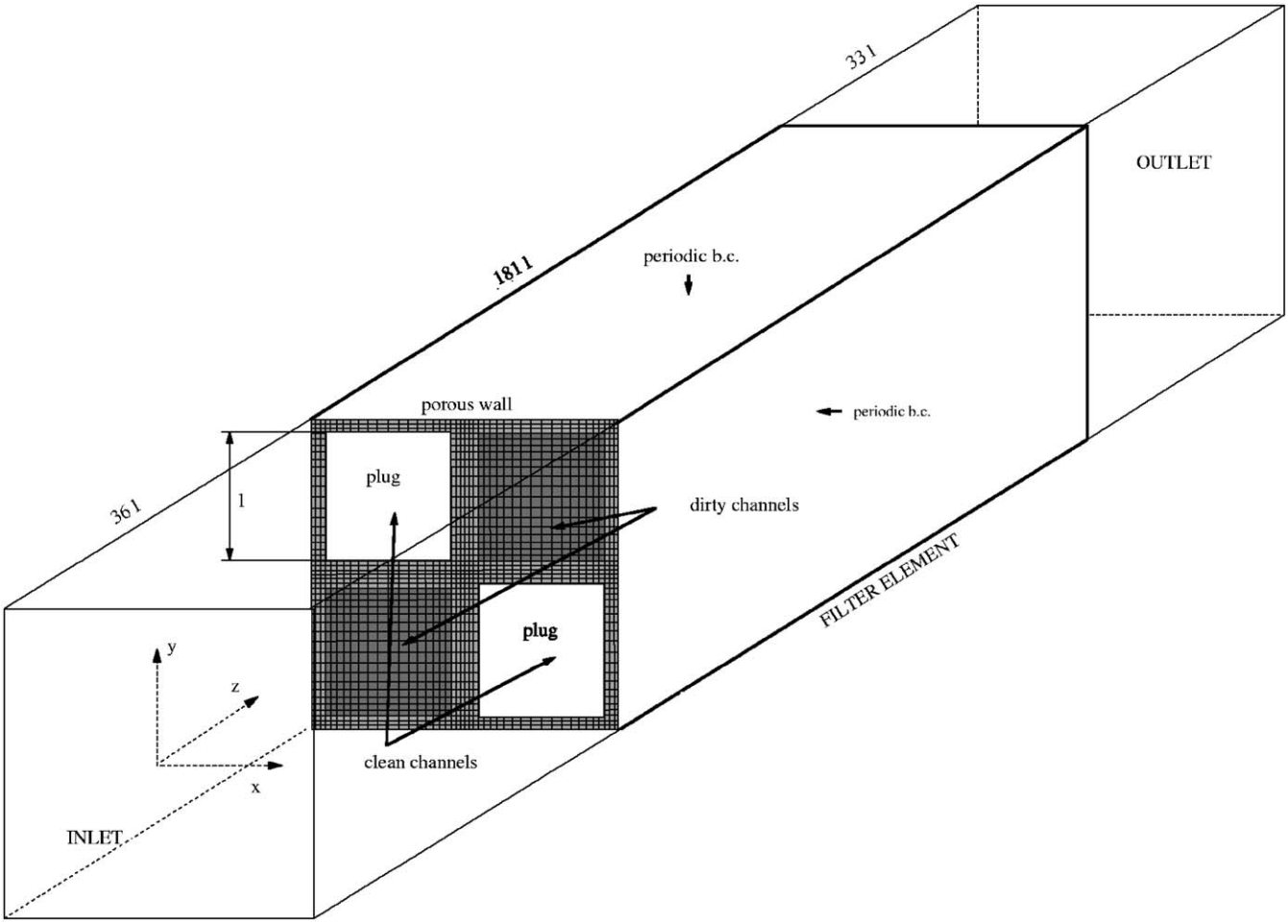

Fig. 2. Axonometric view (mesh) of four channels which form the elementary filtration cell, modelled via a finite-volume CFD code for the solution of the Navier–Stokes equation (Star-CD).

equation (6) is used.

$$\frac{\mathrm{d}p}{L} = \frac{-150\mu(1-\varepsilon)^2 u}{\varepsilon^3 D_p^2} - \frac{1.75\rho(1-\varepsilon)u^2}{\varepsilon^3 D_p}. \tag{6}$$

Here, μ is the fluid molecular viscosity and D_p is the average diameter of the grains forming the porous medium. Combining Eqs. (5) and (6) we obtain

$$\alpha = \frac{1.75\rho(1-\varepsilon)}{\varepsilon^3 D_p}; \quad \beta = \frac{150\mu(1-\varepsilon)^2}{\varepsilon^3 D_p^2}. \tag{7}$$

To determine α and β we need thus, other than the values of ρ, μ and ε, the average diameter of the grains D_p, which is a priori unknown. The uncertainty in the average value of D_p (observed through microscope) leads to large errors in the determination of α and β. For this reason, we took an average value of D_p from literature only to perform a first simulation—with trial values of α and β—which purpose was that of giving us a starting point from which to proceed for further adjustment of D_p to fit with the experimental value of pressure loss at given values of the mass flowrate. Experiments were performed to measure the characteristic pressure—flowrate velocity curve and data are provided in Section 3.

2.4. Sub-micron particle modelling

To simulate the behavior of particles with dimensions smaller than 1 μm (sub-micron particles) we must account for the non-continuous molecular structure of the flow. It is known (Li and Ahmadi, 1993; Crowe et al., 1998) that for particles having dimension smaller than the mean free path of the molecules of the gas in which they are dispersed, the carrier fluid is far from being a continuum, since it interacts with particles as a collection of rigid bodies which randomly collide with the particle, with intensity depending on the kinetic energy content of the molecules (i.e., on the gas absolute temperature). This introduces two effects: (i) a Brownian force term able to modify particle trajectories in a nearly random fashion and (ii) a partial slip, which reduces the drag coefficient depending on dilution parameters. The parameter used to quantify dilution effect is the Knudsen number, defined as the ratio of the mean free path of the gas

molecules λ and the particle diameter d_p:

$$Kn = \frac{\lambda}{d_p}. \tag{8}$$

The mean free path of a molecule can be calculated from kinetic theory by (Sharipov and Seleznev, 1998):

$$\lambda = \frac{\sqrt{\pi}\mu}{2P}\left(\frac{2RT}{m}\right)^{1/2}, \tag{9}$$

where T is the gas temperature in K, d_m is the molecule diameter, m is the molecular mass in atomic units P is pressure and R is the universal gas constant. In the present case, characterized by a temperature of $T = 600$ K, and a pressure of 100 kPa, the mean free path value is (for air) $\lambda \cong 1.040 \times 10^{-7}$ m. The value of the Knudsen number is then $Kn \cong 0.52$ and we are in the case of *transitional flow* (Crowe et al., 1998), defined for $0.25 < Kn < 10$.

We calculated the trajectory of each particle by integrating over time the equation of motion—i.e., using a Lagrangian approach—modelling the particles as non-interacting, non-deformable solid spheres and considering one-way coupling momentum transfer between particles and fluid. Time advancement is done with a forward-Euler method, using a time step of 5.7×10^{-8} s. The small time step is determined by the small size of the particles and makes simulations long and costly. Further improvement may be achieved by using semi-implicit methods.

The generic equation of motion for each particle, written in a Lagrangian reference frame is

$$\rho_p \frac{\pi d_p^3}{6}\frac{\partial \vec{v}}{\partial t} = \sum_i \vec{F}_i, \tag{10}$$

where d_p is particle diameter, ρ_p is particle density and $\vec{v}$ is particle velocity vector. The sum of forces on the RHS of Eq. (10) represents all the forces acting on a particle in a fluid stream. For the purposes of the present work, the assumption of transitional flow described leads to the following expression (Ahmadi and Chen, 1998):

$$\frac{d\vec{v}}{dt} = \frac{3\nu C_D Re_p}{2d_p^2(2\rho_p/\rho + 1)C_c}(\vec{u} - \vec{v}) + \vec{F}_b(t) \tag{11}$$

in which $\vec{u}$ is the fluid velocity at the particle position, ρ is fluid density and C_D is the drag coefficient evaluated as (Ahmadi and Chen, 1998):

$$\frac{24}{Re_p}\left(1 + \frac{1}{6}Re_p^{0.67}\right), \tag{12}$$

Re_p being the particle Reynolds number:

$$Re_p = \frac{d_p|\vec{v} - \vec{u}|}{\nu}. \tag{13}$$

Eq. (12) represents a good approximation for the drag coefficient while $1 < Re_p < 1000$. C_c is the Stokes–Cunningham slip correction, calculated as:

$$C_c = 1 + 2Kn[1.257 + 0.4\ \exp(-0.55Kn)]. \tag{14}$$

The second term on the RHS of Eq. (11) is the Brownian force, which also becomes important for sub-micron particles. This Brownian term was simulated as a Gaussian white noise random process (see Ounis et al., 1991; Gupta and Peters, 1985; Li and Ahmadi, 1993; Ahmadi and Chen, 1998).

To evaluate the overall effect of both transitional flow and of Brownian effect, we performed Lagrangian tracking of two swarms of 0.2 μm particles released at the same initial positions. The first simulation, called *no-slip* case, included only drag and inertia acting on particles; the second simulation, called *slip* case, included also the Cunningham correction factor C_c for drag calculation and the influence of the Brownian term described above.

2.5. Porous wall–particle interactions

During an impact between a particle and a wall, kinetic energy is dissipated (i) via plastic deformation during the particle–wall approach and (ii) through adhesion–separation work during the contraction phase (Johnson et al., 1971; Johnson and Pollock, 1994; Brach and Dunn, 1995, 1998). The material properties both of the particles and of the impacting barrier strongly affect these energy losses, making experimental measurements of crucial importance. In this work we considered the rigid-body impact models developed by Caylor (1993), Dunn et al. (1995) and Brach and Dunn (1995) among others, and kinetic-energy-based models such as that developed by Dahneke (1995).

Dahneke (1995) presented an energy-based model for a simple-collision process in which energy of plastic deformation dissipated during the approach phase, and energy of separation from the adhesive force in the contraction (rebound) phase were accounted for by means of a coefficient of restitution e, which is thus the ratio between the wall-normal component of the approaching velocity v_i and the wall-normal component of the rebound velocity v_r ($e = v_i/v_r$). The coefficient of restitution was validated through normal-impact experiments in which 1.27 μm polystyrene spheres hit a fused-silica surface at different velocities. Starting from the experimental curve of Dahneke (1995), shown in Fig. 3(a) as white circles, we calculated an interpolation function, also shown in Fig. 3(a) with the continuous line, using the following expression for the coefficient of restitution:

$$e = 0.94\left[1 - \exp\left(-\frac{v_i + 0.5}{1.6}\right)\right] + 0.02. \tag{15}$$

This correlation reproduces well the behavior of the coefficient of restitution for the range of incident normal velocities up to 20 m/s, as visible in Fig. 3.

As it will be discussed later, we observed from simulations that wall normal velocities never exceed 0.05 m/s in

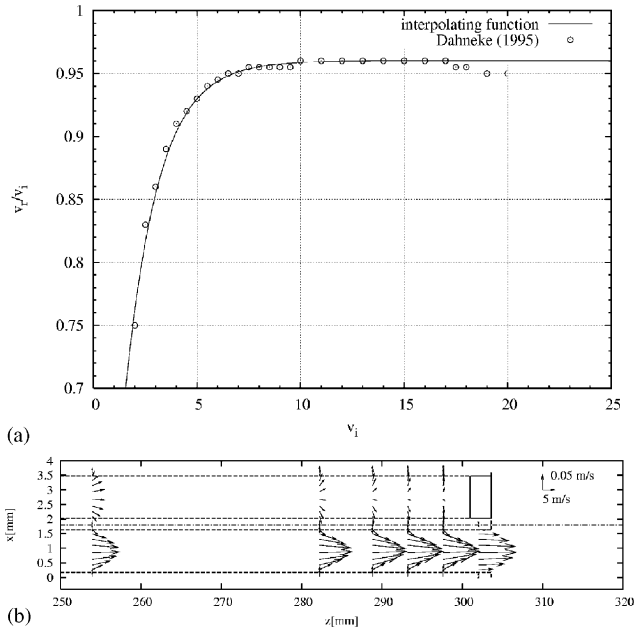

Fig. 3. Interpolation function (a) used to calculate the coefficient of restitution during impacts between soot particles and the porous wall, according to the experimental observations of Dahneke (1995). As visible from the vectorial representation of the velocity field shown in (b), small normal velocities cause very small coefficient of restitution, involving that all particles are captured after an impact.

the entire micro-channel. Again, from Fig. 3, we notice that for normal velocity lower than 2 m/s, the coefficient of restitution has not been experimentally determined, but approximated through an asymptotic expression (Dahneke, 1995) going to zero while normal velocity value decreases. Consequently, we can assume that particles with $v_i \leqslant 2\,\mathrm{m/s}$ are probably all captured by the adhesive forces and by adsorption on the ceramic surface. We verified a posteriori that even applying the bounce–capture model of Dahneke (1995), all particles are captured at their first impact.

3. Results

3.1. Experimental validation

Measuring local velocities in the filter channels without altering the filter geometry is made difficult by fragility and hardness of the materials used. Thus, we made an indirect flow field validation by using the characteristic curve of the filter, experimentally obtained. As characteristic curve we mean here the pressure drop between the two sides of the filter as a function of the overall mass flowrate W. Experiments were performed in the test facility shown in Fig. 1, in which flowrate is measured with a digital flow meter and Δp is measured with two pressure probes placed up- and downstream of the filter and connected to a differential pressure gauge. Results are reported in Fig. 4 as the continuous line.

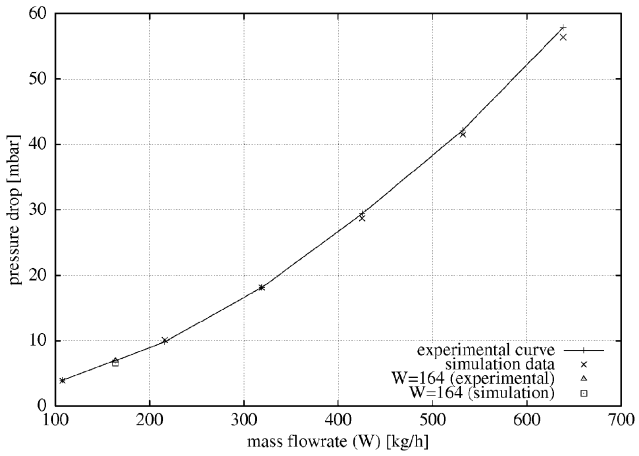

Fig. 4. Comparison between the numerically obtained characteristic curve of the filter (×) and the experimental one (+), used to tune the porosity parameters. Conditions at which soot is released correspond to the point where the mass flowrate value is of 164 kg/h. This point is represented here for the experimental case (△) and for the simulation (□).

To achieve correspondence with experiments, we conducted a set of simulations using the geometry sketched in Fig. 2 and varying the value of D_p (i.e., the average grain size of the porous ceramic) in Eqs. (7). This procedure allows to obtain the permeability coefficients α and β required by the numerical code to impose the porosity conditions (i.e., distributed pressure loss). Simulations were first performed using a tentative value of D_p (found in technical literature) which gave, for the different values of the mass flowrate imposed at inlet (i.e., from 105 to 640 kg/h) an approximate characteristic curve. Using these data, we made successive adjustments of D_p and, by further simulations, we tried to reproduce as accurately as possible the experimental curve. Final result, reported in Fig. 4, shows a good agreement with experiments. To perform Lagrangian tracking, we used instead a fixed mass flowrate of $W = 164\,\mathrm{kg/h}$ ($4.556 \times 10^{-2}\,\mathrm{kg/s}$), included in the interval used to tune porosity parameters. Corresponding point is marked on the characteristic curve of Fig. 4 with different symbols (representing the experimental and the numerical value).

3.2. Fluid velocity profiles

Particle behavior is dominated by the flow field. Specifically, fluid velocity in different regions of the micro-channel may determine differences in particle deposition and trapping, due to locally non-uniform particle flows. Furthermore, the cross-wall flowrate may heavily affect those particles whose dynamics are dominated by the drag force. For this reason, as preliminary observations on the flow field we decided to examine (i) velocity profiles at different z positions along the entire 4-micro-channel filter-element, and (ii) the cross-wall flowrate variations along z coordinate.

We expect the gas flow leaving progressively a dirty channel to be transferred through the porous walls to the adjacent clean channels, giving place to a progressively decreasing mass flowrate in the former and a corresponding increase in the latter while proceeding along the z coordinate. However, we have no experimental evidence on how the cross-wall (or through-wall) flowrate varies along a channel nor on the shape of velocity profiles inside the channels. There are several works on flow in square channels showing presence of counter rotating corner vortices (Gavrilakis, 1992) which may influence particle deposition. However, the porous wall boundary condition changes strongly the velocity distribution and few words are necessary to describe the phenomenon.

In Fig. 5(a), axial velocity profiles in the meridian plane of a pair of complementary channels (dirty channel, below and clean channel, above) are shown. Profiles refer to different values of the z coordinate and more profiles are concentrated at closer z positions where velocity changes are steeper, i.e., at channel inlet and outlet. Shown profiles correspond to an overall flowrate (across the filter section) of 4.556×10^{-2} kg/s (164 kg/h), i.e., to the normal working conditions, characterized by an average velocity over the filter section area of 3 m/s. In the dirty channel, we observe an initially flat velocity profile (close to the inlet section— Fig. 5(a)) that adjusts to a parabolic Poiseuille profile proceeding downstream, with almost constant centerline velocity. At about 80% of the channel length, centerline velocity decreases abruptly. In the clean channel we observe profile variations complementary to those observed in the dirty one, with a slowly increasing parabolic profile which suddenly grows at about 80% of the channel length. Flow rate across the channel walls is thus strongly non-uniform in the axial direction.

In Fig. 5(b) the through-wall flowrate along the pair of channels is shown. Two peaks are visible at the inlet and at the outlet of the channels, respectively, and the amplitude of the peak at outlet is about 1.5 times that of the inlet. The initially flat velocity profiles observed in Fig. 5(a) involve higher near-wall velocities (i.e., an higher near-wall flow) which in turn causes an initially high wall-flow which decreases progressively proceeding along z, as the profile adjusts to Poiseuille parabolic law. On the other hand, a certain pressure rise is observed proceeding toward the plugged end, and it causes a rapid growth of the through-wall flow, producing the second peak. The fluid transfer across the walls of the filter is thus non-uniform and shows a higher peak in correspondence of the final section, a smaller one at the inlet of the channel and a minimum in the middle. This behavior is bound to influence particle deposition along the filter and is partially responsible for non-uniform particle concentrations observed in the deposition process.

3.3. Particle deposition

In the previous sections we have identified some of the main characteristics of the flow field developing in the micro-channels; knowing that these are able to affect particle dispersion and deposition along the channels, we want to identify which ones, among those we cited, play the major role. To this purpose, we examined the behavior of $O(10^4)$ soot-representative particles with density $\rho = 1000\,\mathrm{kg/m^3}$ and diameter ranging from 0.2 to 2 μm. In our simulations gravity is neglected and deposition is controlled by drag and inertia; for this reason density does not enter as a parameter in the particle equation of motion (11) but appears in combination with particle diameter. We run one simulation for a set of larger, 2 μm diameter particles and two distinct simulations for a set of smaller 0.2 μm particles, to examine separately the influence of Brownian motion and of the partial slip with the air molecules accounted by the Cunningham factor. Table 1 reports the data of the three simulations. Aim of these simulations is to verify if there are and which are the locations for preferential particle distribution.

The position at which particle deposit for the three different simulations is shown in Fig. 6. Figs. 6(a)–(c), on the left, show the position at which particles impact on the porous walls. Figs. 6(a)–(c) have been obtained adding the data obtained for each of the four channel sides. Since almost all particles impact the wall with low velocity, this picture is representative of particle deposition probability and thus of soot accumulation in the channel for the 2 μm simulation, for the 0.2 μm slip case and for the 0.2 μm no-slip case, respectively. Figs. 6(d)–(f) represent in a more quantitative way the evolution of particle deposition along the channel length. Figs. 6(d)–(f) show the deposition efficiency and have been computed by integrating particle concentration number along x and y directions for different values of z in a dirty channel. They also represent the probability density function (PDF) of the deposited particle concentration number N/N_0 as a function of the axial coordinate z. From Fig. 6 it is clearly visible that particles preferentially deposit at the end of the channel. This effect is modulated by particle inertia, being more pronounced for the larger particles (see Figs. 6(a) and (b)). This tendency may be explained looking at Fig. 5(b): small particles follow the through-wall flow very closely and reach the wall, where the flowrate is larger, precisely at the end of the channel. Observing Fig. 5(b), we noticed a large wall flowrate at the channel inlet. However, virtually no particle deposit at the channel inlet due to inward effect: particle paths bend after the inlet and reach a condition of *vena contracta* (not shown here) which brings particle trajectory farther from the wall. Examining Figs. 6(a)–(c), we notice that smaller 0.2 μm particles deposit more uniformly on the channel walls, compared to the larger 2 μm particles. Smaller and larger particles share the general trend to deposit along the corners. The dashed line in Figs. 6(d)–(f) represents the rescaled shape of the through-wall velocity profile shown in Fig. 5(b). The behavior of the through-wall flow is qualitatively very similar to particle deposition efficiency only in the second half of the channel. This indicates that not only the through-wall flowrate

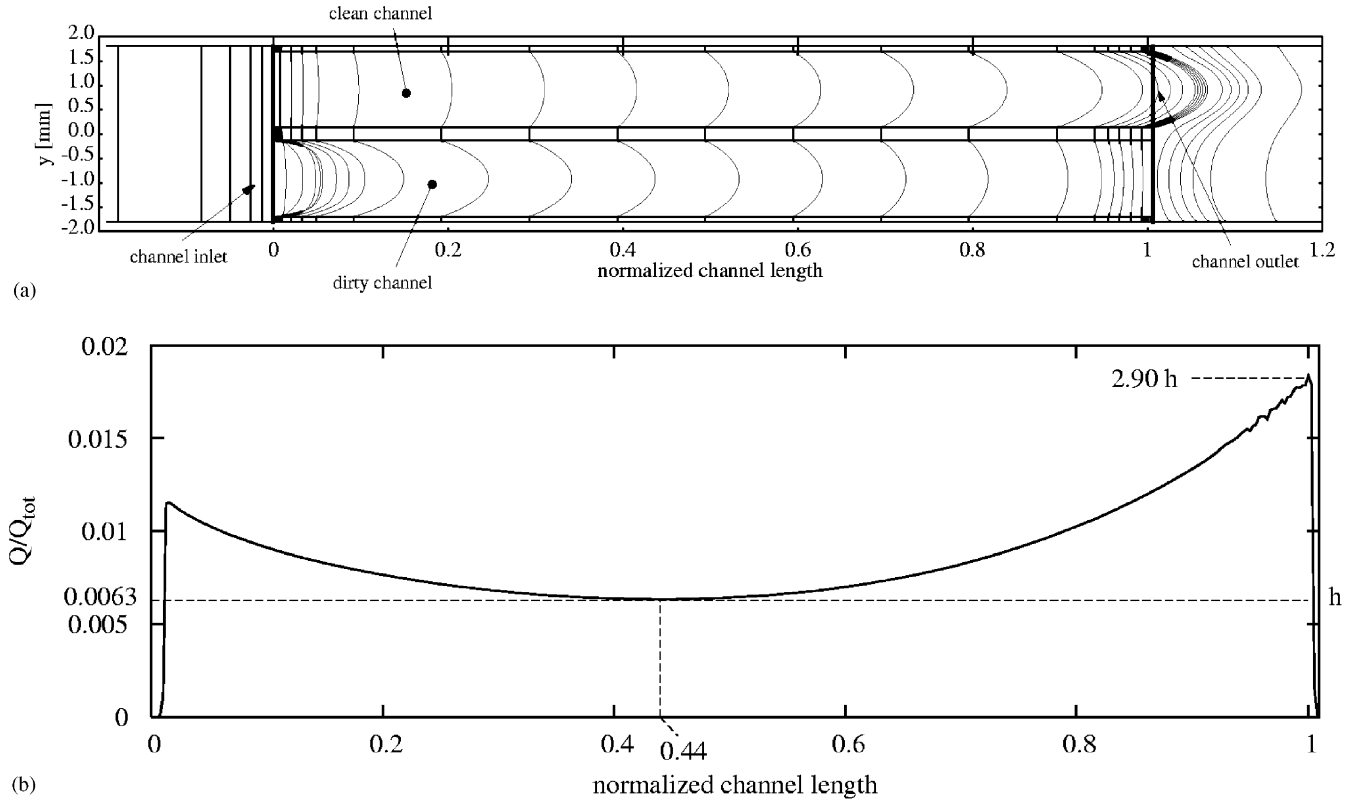

Fig. 5. Axial-velocity profiles along two adjacent channels of the filter (a) and normalized flowrate across the wall along z coordinate (b).

Table 1
Particle parameters and forces considered in Lagrangian tracking simulations

Simulation no.	ρ_p (kg/m^3)	Forces	d_p (m)	τ_p (s)
I	1000	drag, inertia	2×10^{-6}	1.15×10^{-5}
II	1000	drag, inertia	2×10^{-7} (no-slip)	1.15×10^{-7}
III	1000	drag+slip, inertia, Brownian	2×10^{-7} (slip)	1.15×10^{-7}

controls particle deposition, but also the *vena contracta* condition, which causes particle paths to bend inward, preventing deposition in the initial part of the channel. It is interesting to notice that the rapid increase of the through wall flowrate in the final part of the channel—due to pressure rise in correspondence of the plug—is the cause of higher deposition observed here.

It is interesting now to examine the influence of the Brownian motion and of the Cunningham slip factor on particle deposition. Observing Figs. 6(b) and (e) against Figs. 6(c) and (f) we hardly notice any difference which shows a clear trend. We thus examined the trajectory of single particles released from the same position in the two cases of no Brownian motion and no-slip, and with Brownian motion and slip. We plot the trajectory of twelve selected particles in Fig. 7. We chose particles which deposit in different locations along the channel wall. Lines refer to the no Brownian motion and no-slip case, whereas symbols refer to the Brownian motion and slip case. We notice slight differences but randomly distributed. For instance, in case 1 and 12 particles deposit farther in the slip case, whereas they deposit nearer in cases 2 and 6.

For filter design optimization, it is very important to quantify global different behavior of the different size particles (0.2 and 2 μm particles) and for the different modelling approaches (Brownian and slip, or not). We try to do this comparison in Fig. 8, where we show the differences in the deposition location for the three cases examined. Fig. 8(a) is computed by subtracting the deposition PDF for the 0.2 μm no-slip case from the deposition PDF for the 2 μm case; Fig. 8(b) is computed by subtracting the deposition PDF for the 0.2 μm slip case from the deposition PDF for the 2 μm case, and Fig. 8(c) is computed by subtracting the deposition PDF for the 0.2 μm slip case from the deposition PDF for the 0.2 μm no-slip case. Figs. 8(a) and (b) are largely similar, indicating that smaller particles tend to deposit more

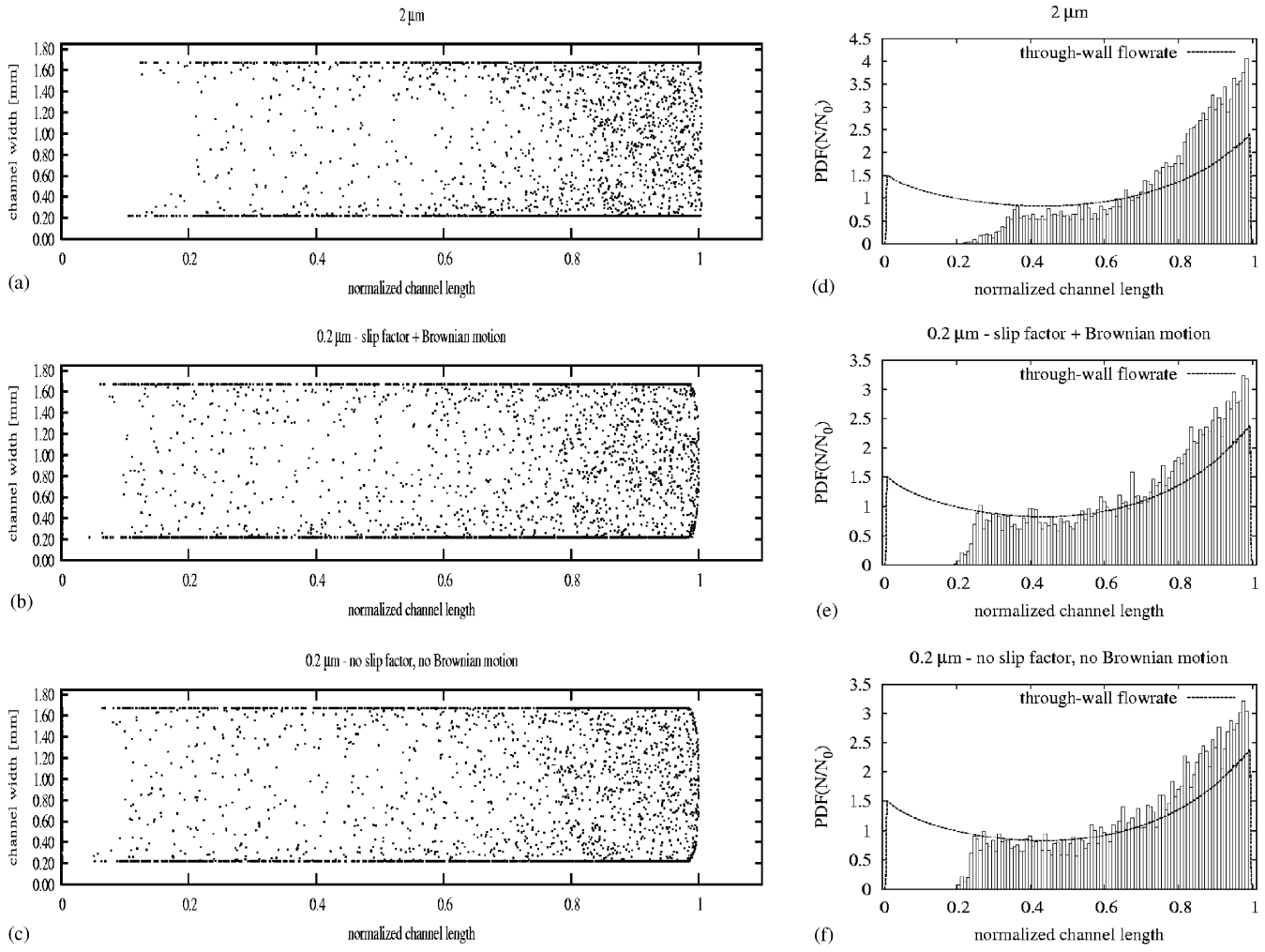

Fig. 6. Particle accumulation and probability density function of particle concentration number inside the filter dirty channel. Lagrangian tracking of $O(10^4)$ particles was used. Dispersions shown refer to soot particles of 2 μm (a) and 0.2 μm (b) and (c) diameter, respectively. Cunningham slip factor and the effects of Brownian motion are taken into account for the 0.2 μm particles in (b) only.

preferentially in the initial part of the channel compared to the larger particles. In Fig. 8(c) we observed no distinct trend, indicating that slip and Brownian motion are just random noise to particle deposition (difference distribution in Fig. 8(c) is in fact similar to a white noise random distribution, such as that used to model Brownian term—Li and Ahmadi, 1993).

In Fig. 9 we show the correlation between the through-wall fluid velocity and particle preferential deposition. Point-line profiles shown in Fig. 9(a) demonstrate the local through-wall flowrate measured at 5 different positions along the channel, corresponding to 20%, 40%, 60%, 80% and 100% of the channel length, respectively. Histogram representation of Figs. 9(b)–(d) show the particle concentration number, measured at the same positions of Fig. 9(a), for the 2 μm particles (b) and for the 0.2 μm particles slip case (c) and no-slip case (d). Axis z is parallel to the channel axis, as shown in Fig. 2 and quantities are evaluated along the x direction (corresponding statistical quantities evaluated along the y direction will give the same values). The x coordinate is normalized through the channel side l and, due to the symmetry of domain, only half of the channel is represented in the figure.

Fig. 9(a) shows that the through-wall flowrate has a peak in correspondence of the corner area, where higher particle concentrations are also observed, as visible in Figs. 9(b)–(d). The presence of an higher wall flowrate in correspondence of the corner can be explained by considering that, being through-wall flow a function of the pressure difference across the wall, broadly constant in the spanwise direction, furthermore being the region of the corner adjacent to two clean channels, wall-normal velocity vectors in correspondence of a corner are given by the sum of the x and y components. For this reason higher wall-normal velocities are present in this region and cause higher wall flowrate (and higher deposition).

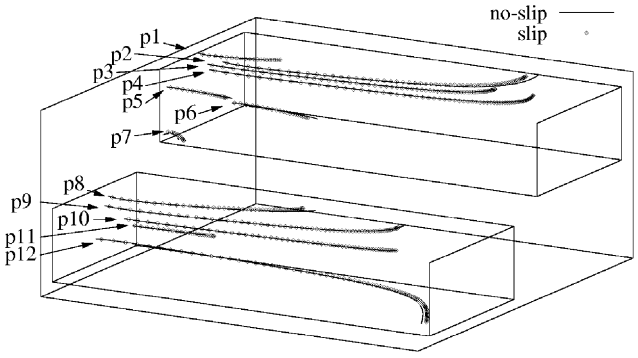

Fig. 7. Sample of twelve 0.2 μm particle trajectories (p1–p12) showing the effect of the Cunningham slip factor and of the Brownian term on particle trajectories. Particles are released at the same position—with velocity equal to that of fluid in the same point—for two independent simulations with different assumptions, i.e., one neglecting the two terms (no-slip case) and accounting for Stokes drag and inertia only, and the other (slip case) accounting for the Cunningham correction factor in the drag coefficient and the Brownian term.

3.4. Discussion on the influence of Brownian term

It is known (see, e.g., Chang and Whang, 1997; Chinju et al., 2001; Chang et al., 2002; Kim and Zydney, 2004 among others) that the influence of the Brownian term in the deposition process of particles with size smaller than $O(1)$ μm becomes important. Specifically, Brownian diffusion is the fundamental mechanism by which particles are captured on solid surfaces, e.g., in the viscous sublayer of a boundary-layer, where streamlines are parallel to the wall boundary, as sketched in Fig. 10 (a). As shown in Fig. 10(a), different inertia particles deposit following three distinct mechanisms: (A) inertial impact, dominating the deposition process of the larger inertia particles; (B) interception, which play a role for intermediate inertia particles and (C) Brownian diffusion, that becomes important for sub-micron particles, which otherwise tend to slip over the solid boundary. An aerosol particle under the effect of the drag force (and inertia) only, due to its small inertia, tend to follow the wall-parallel streamlines of the viscous sublayer and there is no reason for it to hit the wall, unless a transverse force, such as the random Brownian motion, is applied. In the case of the micro-porous filter channels object of this paper, even though particles are very small we found the Brownian effect negligible on particle deposition. The explanation for this fact is found on the specific flow configuration encountered in this type of problem, in which streamlines are not parallel to the solid surface (actually, a porous surface which is seen as a solid wall for the particles but as a permeable medium for the flow) but generally they cross it. Separation mechanism for the present flow configuration is thus different from that found in case of non-porous walls shown in Fig. 10(a), and is sketched in Fig. 10(b). As we can note from this figure, particles follow the streamlines with distorted path-lines because the Brownian effect. However, since streamlines cross the ‘solid’ boundary, the effect of the Brownian term is a “random” shift in the impacting location, substantially not able to affect final particle concentration from a macroscopic viewpoint. For this reason, in the case of particle-laden flow crossing a porous medium presented here, even if transported particles are in the

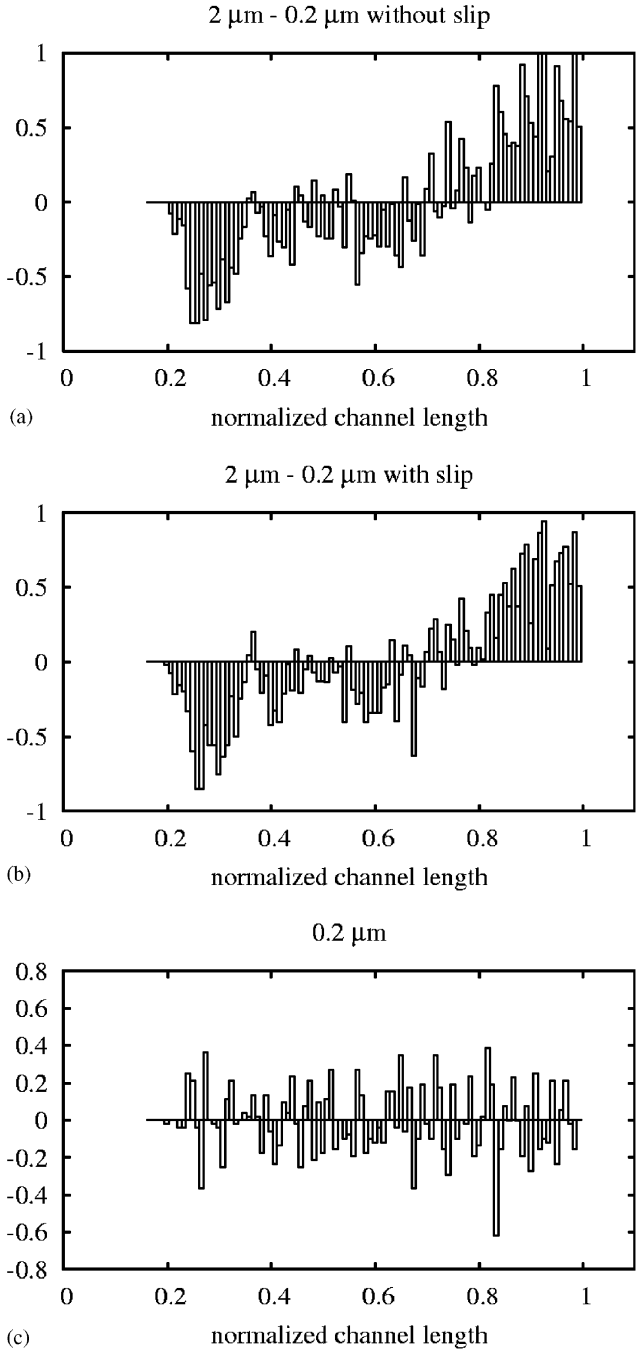

Fig. 8. Difference between the probability density function of particle concentration numbers reported in Figs. 6(a)–(c), measured along the channel. Difference between 2 μm PDF and two different 0.2 μm PDFs are reported in (a) and (b); (c) shows the difference between the two 0.2 μm PDFs.

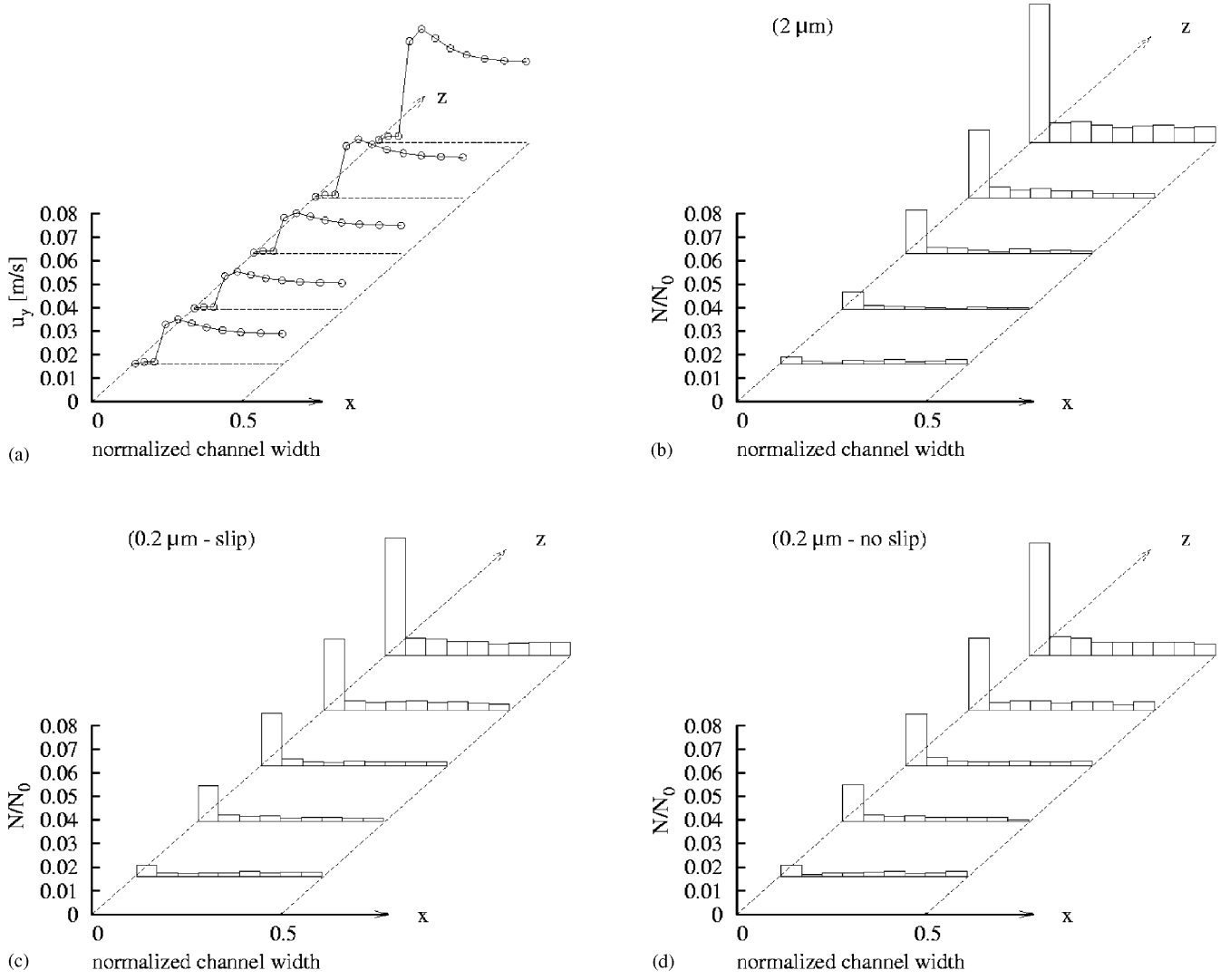

Fig. 9. Through-wall velocity profile (a) and deposition of particles on the walls in correspondence of 5 different portions of a dirty micro-channel. The three different particle sets are: (b) 2 μm; (c) 0.2 μm *slip* case; (d) 0.2 μm *no-slip* case. Velocity and concentration profiles refer to 20%, 40%, 60%, 80% and 100% of the channel length, respectively.

sub-micron range, we can assume that drag and possibly inertia still dominate particle deposition.

4. Conclusions

The soot produced by diesel engines is characterized by particles having diameter of $O(10^2\,\text{nm})$, i.e., being part of the so-called PM10 and PM2.5, which are possibly responsible for lung-damaging and carcinogenic effects (Saracco et al., 1999; Kagawa, 2002; Fino et al., 2003). To reduce emissions of such pollutants, porous-ceramics-based particulate filters are employed in the exhaust line of vehicles. In the present work, a numerical approach to investigate the behavior of sub-micron diesel soot particles in the micro-channels of a wall-flow-type filter is presented.

A lack of literature on theoretical approaches to particulate filtration by means of porous materials exist, and few numerical approaches describing the dispersion mechanisms for sub-micron particles are available both in wall-flow and in other types of filter. We thus chose to model particle behavior through a Lagrangian approach, using the flow field obtained by a commercial finite-volume Navier–Stokes solver (Star-CD) and validated through experimental data, measured on a recent type of silicon carbide (SiC) filter. The Ergun equation has been used to model the porous material of the filter and porosity parameters were fitted to obtain the best agreement with experimental data, in terms of pressure loss.

Lagrangian approach is a suitable way to model particle behavior and to introduce specific terms in the equation of motion, such as the Cunningham correction factor (slip factor) for the drag coefficient and a Brownian force term,

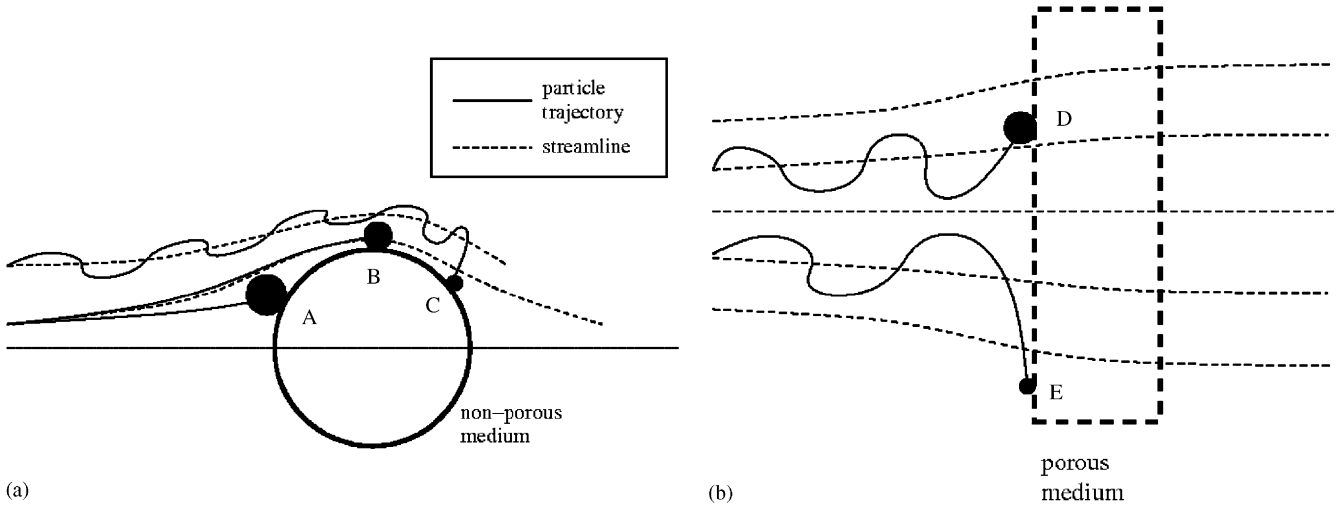

Fig. 10. Influence of the Brownian term in sub-micron particle capture process on non-porous surface (a) and porous surface (b).

which becomes important for Knudsen numbers higher than 0.25 (Crowe et al., 1998). Furthermore, Lagrangian approach is the most natural way for the application of bounce/capture models during the impact phase between particles and solid walls, being these latter usually based on the kinetic energy loss involved during the (two) phases of an impact event (Caylor, 1993; Dunn et al., 1995; Brach and Dunn, 1995; Dahneke, 1995). In the present work, using the experimental data of Dahneke (1995) we defined an interpolation function for the value of the restitution coefficient *e*, as a function of the approaching velocity, we used in our Lagrangian tracking simulations.

After validation of the flow field obtained through validation of the experimental characteristic curve of the filter, we were able to investigate in detail local velocity values and profiles. We found that axial velocity profiles—after an adjustment in the initial portion of the channel—are laminar and follow the parabolic Poiseuille law. The centerline velocity characterizing such profiles reduces progressively while proceeding along the channel, due to the through-wall flow, i.e., the fluid flow rate that moves to adjacent channels due to the presence of alternately arranged plugs, placed either at the end or at the beginning of each channel. The flowrate transfer across the porous walls is not constant along the axis, and shows two maxims at channel inlet and at channel end. The minimum flowrate is observed in the middle (50% of the channel length).

Non-uniformity in the through-wall flow causes non-uniformity in particle deposition which follows quite faithfully the through-wall flow trend starting from an axial position which varies along the filter axis depending on particle inertia. Two different particle diameters were considered for Lagrangian tracking, i.e., 2 and 0.2 μm; due to inertial effects, particle capture begins, for the small particles at about 0.2 times the channel length and at about 0.4 times the channel length for the larger particles. Deposition increases while proceeding downstream, following the through-wall flow behavior. Larger 2 μm particles require larger through-wall flow rates to deposit and reach in larger amounts the channel end. According to our simulations, 50% of the larger particles deposit within 80% and 100% of the channel length. Due to smaller inertia, 0.2 μm particles deposition is more uniform along the filter since they are able to follow the through wall flow even in the central part of the channel, where it is weaker. Nearly no particles deposit in the initial portion of the channel. Non-uniformity in particle deposition process is observed also in the spanwise directions since the through-wall flowrate peaks in correspondence of the channel corners. A peak of particle deposition is observed thus in correspondence of the channel corners both for the 2 μm and for the 0.2 μm particles.

To evaluate the effect of dilute flow hypothesis in Lagrangian tracking of sub-micron particles we made two distinct simulations of the 0.2 μm particles, one accounting for the influence of Brownian motion and of the partial slip with the gas molecules accounted by the Cunningham factor, and the other neglecting them. By comparing the results of these two simulations we found that the dilute flow terms are able to affect particle concentration and deposition only locally, in a random fashion, but they have no effect, from a statistical viewpoint, on final particle deposition. This is due to the fact that the present flow configuration, differently from those cases involving the presence of a viscous sublayer with streamlines parallel to the solid wall boundary (Soldati, 2005), is characterized by streamlines which cross the wall. Thus, particles are only locally deviated from an undisturbed (i.e., streamline-close) trajectory and the result on final concentrations is negligible.

Acknowledgements

Support to this work by the "Centro Ricerche Fiat" of Orbassano (TO - ITALY) is gratefully acknowledged. One author (FS) thankfully acknowledges ATA (Associazione Tecnica dell'Automobile) for support during this research.

References

Ahmadi, G., Chen, Q., 1998. Dispersion and deposition of particles in a turbulent pipe flow with sudden expansion. Journal of Aerosol Science 29 (9), 1097–1116.

Ambrogio, M., Saracco, G., Specchia, V., 2001. Combining filtration and catalytic combustion in particulate traps for diesel exhaust treatment. Chemical Engineering Science 56, 1613–1621.

Ambrogio, M., Saracco, G., Specchia, V., van Gulijk, C., Makkee, M., Moulijn, J.A., 2002. On the generation of aerosol for diesel particulate filtration studies. Separation and Purification Technology 27, 195–209.

Brach, R.M., Dunn, P.F., 1995. Macrodynamics of microparticles. Aerosol Science and Technology 23, 51–71.

Brach, R.M., Dunn, P.F., 1998. Models of rebound and capture for oblique microparticle impacts. Aerosol Science and Technology 29 (5), 379–388.

Caylor, M.J., 1993. Ph.D. Dissertation, University of Notre-Dame, Notre-Dame, IN, USA.

Chang, Y.-I., Whang, J.-J., 1997. Theoretical simulation of the collection efficiencies of brownian particles. Colloids and Surfaces A 125, 137–148.

Chang, Y.-I., Chen, S.-C., Chern, D.-K., 2002. Hydrodynamic field effect on brownian particles deposition in porous media. Separation and Purification Technology 27, 97–109.

Chinju, H., Nagasaki, S., Tanaka, S., Sakamoto, Y., Takebe, S., Ogawa, H., 2001. Effect of flow field on colloid deposition in filtration process of polystyrene latex particles through columns packed with glass beads. Journal of Nuclear Science and Technology 38 (8), 645–654.

Crowe, C., Sommerfeld, M., Tsuji, Y., 1998. Multiphase Flows with Droplets and Particles. CRC Press, Boca Raton, FL, USA.

Dahneke, B., 1995. Particle bounce or capture search for an adequate theory: I. Conservation-of-energy model for a simple collision process. Aerosol Science and Technology 23 (1), 25–39.

Dunn, P.F., Brach, R.M., Caylor, M.J., 1995. Experiments on the low-velocity impact of microspheres with planar surfaces. Aerosol Science and Technology 23, 80–95.

Fan, F.-G., Ahmadi, G., 1995. Analysis of particle motion in the near-wall shear layer vortices—application to the turbulent deposition process. Journal of Colloid and Interface Science 172, 263–277.

Fan, F.-G., Ahmadi, G., 2000. Wall deposition of small ellipsoids from turbulent air flows—a Brownian dynamics simulation. Journal of Aerosol Science 31 (10), 1205–1229.

Fino, D., Fino, P., Saracco, G., Specchia, V., 2003. Innovative means for the catalytic regeneration of particulate traps for diesel exhaust cleaning. Chemical Engineering Science 58, 951–958.

Gavrilakis, S., 1992. Numerical simulation of low Reynolds number turbulent flow through a straight square duct. Journal of Fluid Mechanics 244, 101–112.

Gupta, D., Peters, M.H., 1985. Journal of Colloid and Interface Science 104, 375.

Johnson, K.L., Kendall, K., Roberts, A.D., 1971. Proceedings of the Royal Society of London A 324, 301–313.

Johnson, K.L., Pollock, H.M., 1994. The role of adhesion in the impact of elastic spheres. Journal of Adhesion Science Technology 8 (11), 1323–1332.

Kagawa, J., 2002. Health effects of diesel exhaust emissions—a mixture of air pollutants of worldwide concern. Toxicology 181–182, 349–353.

Kim, M.-m., Zydney, A.L., 2004. Effect of electrostatic, hydrodynamic, and Brownian forces on particle trajectories and sieving in normal flow filtration. Journal of Colloid and Interface Science 269, 425–431.

Li, A., Ahamadi, G., 1993. Deposition of aerosols on surfaces in a turbulent channel flow. International Journal of Engineering Science 31, 435–451.

Ounis, H., Ahmadi, G., McLaughlin, J.B., 1991. Brownian diffusion of sub micron particles in the viscous sublayer. Journal of Colloid and Interface Science 147, 233.

Saracco, G., Badini, C., Specchia, V., 1999. Catalytic traps for diesel particulate control. Chemical Engineering Science 54, 3035–3041.

Sbrizzai, F., Verzicco, R., Pidria, M.F., Soldati, A., 2004. Mechanisms for selective radial dispersion of microparticles in the transitional region of a confined turbulent round jet. International Journal of Multiphase Flow 30, 1389–1417.

Shams, M., Ahmadi, G., Rahimsadeh, H., 2000. A sublayer model for deposition of nano- and micro-particles in turbulent flows. Chemical Engineering Science 55, 6097–6107.

Sharipov, F., Seleznev, V., 1998. Data on internal rarefied gas flows. Journal of Physical and Chemical Reference Data 27 (3), 657–706.

Soldati, A., 2005. Particles turbulence interactions in boundary layers. Zamm-Zeitschrift fur Angewandte Mathematik und Mechanik 85, 683–699.

Wall, S., John, W., Wang, H.-C., 1990. Measurement of kinetic energy loss for particles impact surfaces. Aerosol Science and Technology 12, 926–946.